UC Irvine

UC Irvine Electronic Theses and Dissertations

Title

Stereolithographic 3D-Printed Pneumatic Digital Logic

Permalink

https://escholarship.org/uc/item/4sb4c6xx

Author

Thai, Chung

Publication Date

2024

Peer reviewed|Thesis/dissertation

eScholarship.org Powered by the California Digital Library
University of California

UNIVERSITY OF CALIFORNIA,
IRVINE

Stereolithographic 3D-Printed Pneumatic Digital Logic

THESIS

submitted in partial satisfaction of the requirements
for the degree of

MASTER OF SCIENCE

in Biomedical Engineering

by

Chung Xuan Thai

Thesis Committee:
Associate Professor Elliot Hui, Chair
Chancellor's Professor Abraham Lee
Associate Professor James Brody

2024

© 2024 Chung Xuan Thai

TABLE OF CONTENTS

LIST OF FIGURES

LIST OF TABLES

ACKNOWLEDGEMENTS

I would like to express my gratitude to my committee for their support and guidance: Dr. Elliot Hui, my committee chair, Dr. Abraham Lee, and Dr. Jim Brody. I sincerely appreciate Dr. Elliot Hui for providing me with learning opportunities and hospitality throughout my time in Hui Lab. Without Dr. Elliot Hui's guidance, this thesis would have been unfeasible.

I cannot thank my mentor enough, Dr. Siavash Ahrar, for his endless support and kindness. Dr. Siavash Ahrar's insightful input and suggestions were essential to the success of this research. Dr. Siavash Ahrar's dedication and confidence in me provided the motivation that I desperately needed.

I thank my family for their continued emotional support and affection during the last two years. To my family, I will not let you down.

ABSTRACT OF THE THESIS

Stereolithographic 3D-Printed Pneumatic Digital Logic

by

Chung Thai

Master of Science in Biomedical Engineering

University of California, Irvine, 2024

Associate Professor Elliot Hui, Chair

In this work, pneumatic digital logic systems (i.e., gates, ring oscillators, and peristaltic pumps) were demonstrated using high-resolution (20 μm) stereolithographic (SLA) 3D printing. Pneumatic digital logic systems are Boolean circuits that use pressure (instead of electricity). To this end, normally closed pneumatic membrane valves are configured analogous to NMOS transistors. Vacuum pressure represents logic "1" or True, while atmospheric pressure represents logic "0" or False. Using three alternative fabrication methods (CNC milling, photolithography, and laser-cutting), pneumatic digital circuits have been built to provide embedded control for physical systems (e.g., microfluidics and robotics). However, scaling and high-aspect-ratio manufacturing of these integrated circuits have remained difficult despite progress. Additive manufacturing (i.e., SLA 3D printing) is attractive for the high-aspect-ratio and scalable manufacturing of pneumatic digital systems. Utilizing the versatile design of SLA 3D printing, circuit density of 3D-printed pneumatic ring oscillators was increased to approximately 7 gates per cm^2, constraining complex pneumatic digital systems and eliminating off-chip controllers. Utilizing a 3-ring pneumatic oscillator to integrate a peristaltic pump, a liquid pump rate as

high as 12 μL/sec was successfully demonstrated. In addition, a set-up that could support prolonged automated fluid experiments was implemented. Advances in SLA prototyping of pneumatic digital logic are strongly encouraged to facilitate futuristic microfluidic applications.

Introduction

Miniaturized microfluidic chips require large external controllers for their operation [1]. In the absence of embedded controllers, integrated valved microfluidics applications have remained in specialized laboratories. Pneumatic digital logic is an attractive approach for the embedded control of integrated microfluidics.

In one approach, normally closed pneumatic membrane valves can be configured analogously to NMOS transistors to create a variety of circuits ranging from ring oscillators, counters, and finite-state machines [2]. Rapid prototyping and manufacturing of these systems remains an active area of investigation. Specifically, advances in additive manufacturing (i.e., stereolithography 3D printing) could provide a rapid approach to prototyping and manufacturing systems with sufficient density and complexity for control of embedded microfluidics.

CHAPTER 1: Pneumatic Logic Manufacturing

Four primary manufacturing methods are well-established for developing pneumatic digital circuits: wet etch, soft-lithography, CNC milling, and laser manufacturing. Each approach has its strengths and limitations (Table 1.1). Grover et al. pioneered the first generation of pneumatic valves using chemical wet-etching of glass substrates [3]. The glass wet-etch has enabled many systems, including ring oscillators, pumps, integrated fluid handling systems, and embedded control circuits (adders, counters, and finite state machines) [4]. The glass wet-etch fabrication approach is robust. Glass is a suitable substrate for many chemical reactions. Additionally, the glass and silicone membrane used in the valve have good adhesion without needing any chemical adjustment. The wet etch approach, however, produces a uniform depth of cut across the glass substrate, thus limiting the gate density (defined as a single valve and the associated pneumatic resistors) that can be achieved. Specifically, the average gate density for this process has been estimated at 2 gates per cm^2 [5]. In the second approach, Devaraju et al. used multi-height soft lithography to achieve densities as high as 4 gates per cm^2 [6]. However, the process required mask alignment, access to cleanroom, and multi-step lithography. In the third approach, Duncan et al. used precision milling of thermoplastics to demonstrate ring oscillators and counters and precision as high as 36 gates per cm^2 [5]. However, this CNC method required the alignment of delicate cutting tools and polished plastic surfaces. Hoang et al. used a similar CNC milling approach to build larger pneumatic valves and ring oscillators to control physical systems beyond microfluidics, including (soft robots) [7]. Their method approached 1.5 gates per cm^2. Following the rapid prototyping strategies, Werner et al. used laser manufacturing (engraving channels and cutting materials) to

develop pumps and droplet generators [8]. Laser manufacturing's gate density approached 3 gates per cm^2 from approximation using ImageJ (National Institutes of Health). Laser manufacturing's gate density was lower than that of the CNC milling; however, the critical advantage of this approach was the rapid prototyping (e.g., 30 iterations in one design cycle). Indeed, CNC and laser manufacturing are effective at achieving multi-depth channels. However, both processes are serial compared to the parallel lithographic approaches. In this investigation, the use of stereolithographic 3D printing was sought as a rapid and simple approach to developing pneumatic digital logic. SLA 3D-printing provided both the desirable multi-depth and parallel manufacturing.

Table 1.1. Current Manufacturing Methods of Pneumatic Logic

	Advantages	Disadvantages	Gates per cm^2
Glass wet etching	good material properties	uniform depth of cut, dangerous chemicals, and cleanroom	2
Soft lithography	high resolution	access to cleanroom, multi-step	4
CNC micro milling	multi-depth of cut, smaller/faster devices	slow fabrication, milling alignment	36
CO_2 laser engraving	fast fabrication, multi-depth of cut	high surface roughness	3
SLA 3D printing	fast fabrication, multi-depth of cut, smaller features than laser etching	difficulty assembling, high opaque	7

Stereolithographic 3D Printing

Stereolithographic 3D printing (SLA) is an additive manufacturing process that uses an ultraviolet (UV) light source to polymerize liquid resin into its solidified form based on prior feature designs. SLA 3D printing is widely used in microfluidics due to its high resolution and versatile material selection. Kamperman et al. utilized SLA 3D printing to manufacture microchannels as small as 50 μm to accomplish 3D parallelization of microfluidic droplet generators [9]. Carnero et al. combined SLA 3D printing with pulsed laser ablation to manufacture a straight micromixer to mix and homogenize chemical reactions [10]. In this manufacturing technique, the UV light is projected onto a platform submerged inside a photopolymer resin tank (Fig 1.1). The printer produces cross-sectional, consecutive layer-by-layer polymerized parts onto the platform. In this investigation, all chips were 3D printed using the microArch S240 (BMF Boston Micro Fabrication) at a print resolution of 20 μm. The material used was HTL (High Temperature Laminating) resin, a methoxy-functional silicone polyester resin with high strength, rigidity, and heat resistance. The printer used a build platform that is 100 × 100 × 75 mm. A clear membrane was used to focus the UV light onto the platform which has a 0.127 mm thickness. For both the platform and membrane, all laser positions at each corner were calibrated to be within 0.020 μm of each other. The scraper for clearing out air bubbles was calibrated to stretch the membrane by 0.05 - 0.1 mm and the roller to straighten the membrane was calibrated to compress the membrane by 0.01-0.02 mm. The overlap of stitch mode was set at 10 pixels. The intensity of the laser was fixed at 62.8 mW/cm^2.

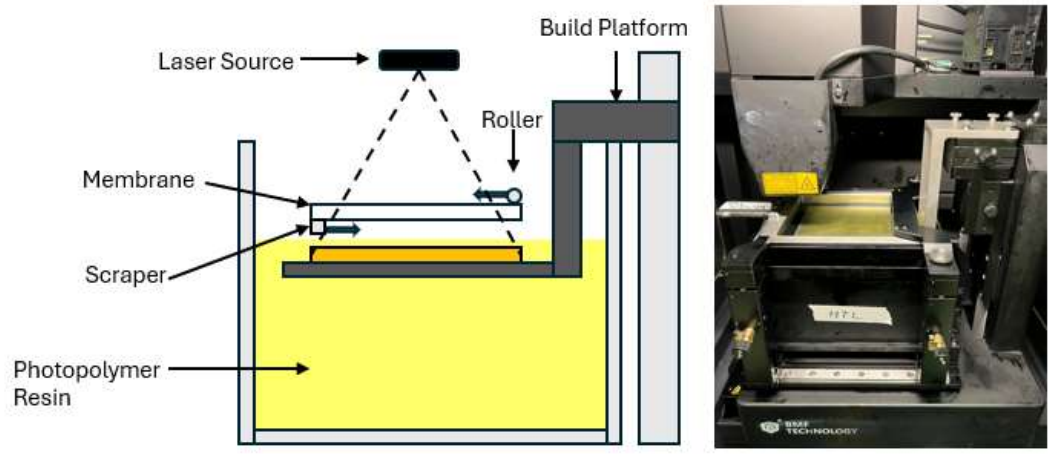

Fig 1.1. Overview of the BMF S230 Printer. The platform is submerged inside a photopolymer resin tank. A laser shines UV light across a transparent membrane to polymerize liquid resin onto the platform.

Chip Design and Manufacturing (Assembly)

All 3D-printed parts were designed via SOLIDWORKS 3D CAD software (Dassault Systèmes SOLIDWORKS Corp.) and converted to Stereolithography (STL) files; a 3D printing file format developed by 3D Systems for stereolithography CAD software. STL files were converted into a series of images through Magics Print for BMF (BMF Boston Micro Fabrication). Each image represented a 20 μm cross-section of the part. Images were exported and transferred to the computer controlling the 3D printer via a USB flash drive. The parts were printed at a resolution of 20 μm in manual stitch mode using the microArch S240 (BMF Boston Micro Fabrication) and HTL resin. After printing, the parts were rinsed in isopropyl alcohol (IPA) for 10 minutes to remove excess uncured resin using Form Wash (Formlabs). The parts were air-dried and then removed from the 3D-printing platform

using a razor blade. The parts were additionally cured for 5 minutes at 45℃ using Form Cure (Formlabs). Before chip assembly for an experiment, each part was first rinsed with DI water and then placed in a Ziploc bag with DI water and microsoap. The Ziploc bags were then sonicated for 20 minutes using the Branson B2510 Ultrasonic Cleaner. After the bath, the parts were rinsed thoroughly with DI water and dried with compressed nitrogen. A 254 μm silicone rubber film (HT-6240, Rogers Corp, Chandler, AZ, USA) was sandwiched between two HTL parts (Fig 2.3A). Via holes, which connect two sides of the parts, were punched at designated locations inside the film using a 2.00 mm punch (Uni-Core Punch, Qiagen Group). The chip was padded with silicone film on both sides. It was then compressed with glass slides on both sides using binder clips and baked for 24 hours at 175℃ in an oven (DX300, Yamato Scientific, Santa Clara, CA, USA10) to promote the adhesion between layers. The chips were allowed to cool down completely before they were removed from the oven for experiments.

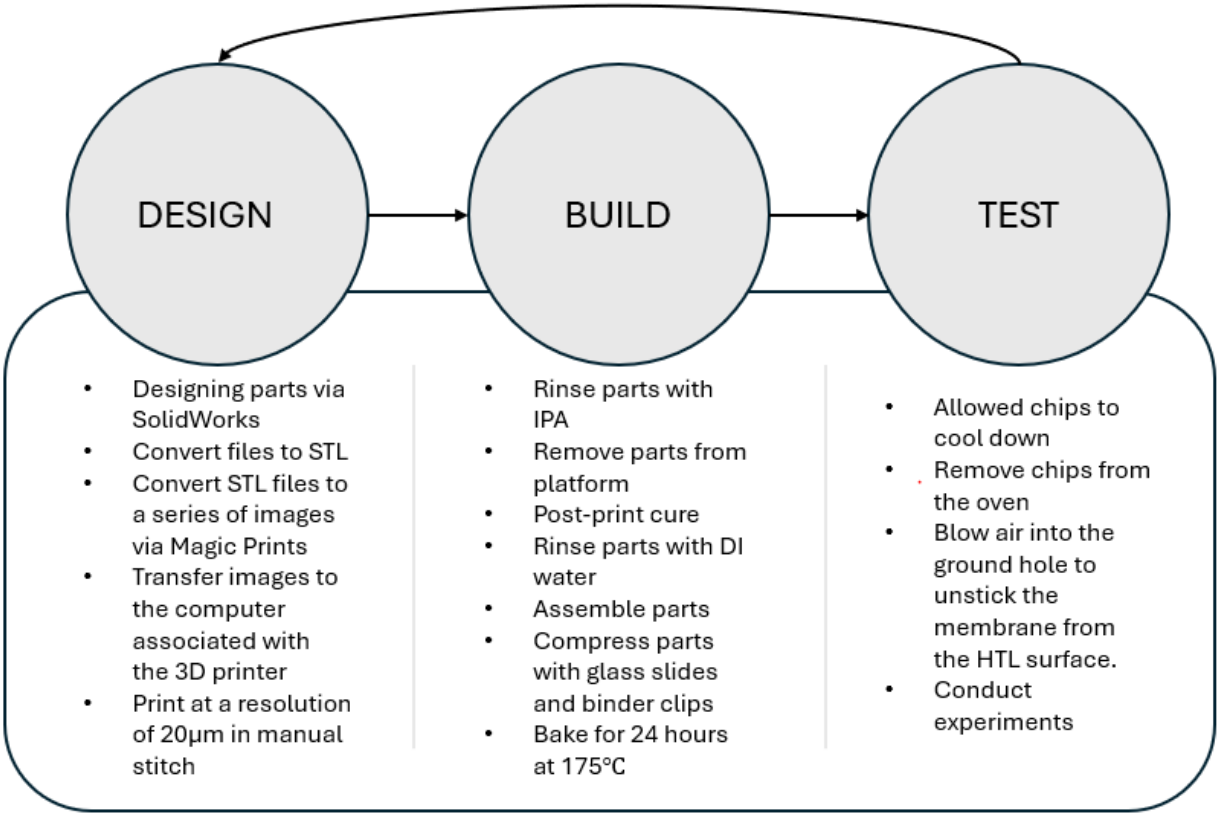

Fig 1.2. Manufacturing Protocols of a Logic Chip. Development of logic chips involves design, build, and test.

CHAPTER 2: Monolithic Pneumatic Digital Logic

In this effort, normally closed pneumatic membrane valves [3] were used as the primary building block of the pneumatic logic circuit. The valve consists of an elastomeric membrane that is embedded in between two parts with channel features (Fig. 2.1A). These pneumatic membrane valves remain closed at rest, blocking the pathway between two pneumatic channels, and actuate when there is vacuum applied to the opposite side of the membrane (Fig. 2.1A). This design can be applied to create a pneumatic inverter gate where there is a high-resistant channel that is connected to the output of the system (Fig. 2.1B). This channel is connected to a constant supply of vacuum (Fig. 2.1B). There is also a channel connected to atmospheric pressure that is separated from the output of the system by the pneumatic membrane valve (Fig. 2.1B). At rest, the valve remains closed, and the output receives vacuum from the resistor channel (Fig 2.1B). The application of vacuum to the input opens the valve, allowing a connection between the output and the ground channel (Fig. 2.1B). Since the ground channel is designed with the least resistance, the output will receive atmospheric pressure instead of vacuum. This mechanism results in the "inverting" of signals, allowing simple controlled output with a single valve. To formalize this behavior, vacuum signals can be defined as digital logic "1" or True, and atmospheric pressure can be defined as digital logic "0" or False. The approach is comparable to n-type metal-oxide-semiconductor (NMOS) logic in electronics, with pneumatic valves being transistors, atmospheric pressure being ground, and resistors being high-resistant pneumatic channels [2].

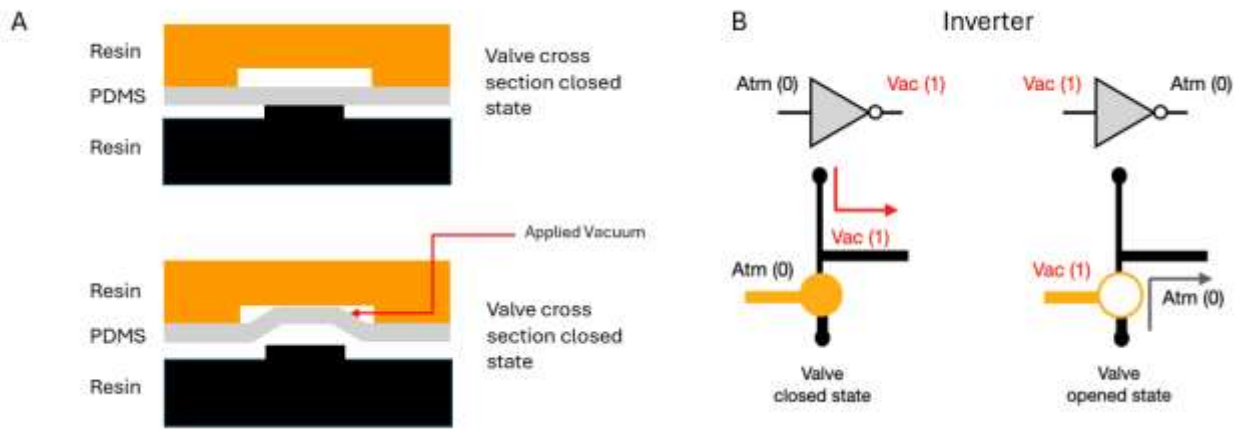

Fig 2.1. Monolithic Valve and Pneumatic Digital Logic. (A) Cross-sectional view of a monolithic valve (orange for the top layer, black for the bottom layer). The top valve is at rest and the bottom valve is actuated. When there is vacuum applied to the control chamber (top layer), the elastomeric membrane (PDMS) is displaced, opening a path between two disconnected channels. **(B)** Operation of a pneumatic inverter. Valve actuation connects the output to atmospheric pressure.

Valve Optimization & Transfer Function Measurements

Using SLA 3D printing, 4 inverter chips were developed. To this end, the operation of four pneumatic valves with diameters 1, 2, 3, and 4 mm was verified. To increase the total gate densities, 1- and 2-mm valves were selected for developing inverters. All inverter chips were designed with an output indicator valve to readily examine their function. The efficacy of an inverter can be determined with the transfer function which quantifies the input/output characteristics. To measure transfer functions, the input was connected to the house vacuum system (WaterSaver Faucet Co.) and the applied pressure was controlled

with a vacuum regulator (V-800-30W/K; AIRTROL) (Fig 2.2). Both the pressure values from input and output were measured using two independent pressure transducers (ASDX Series Silicon Pressure Sensors; Honeywell Solid State Electronics Center) (Fig. 2.2). Values from the transducers were recorded with an Arduino data acquisition system. The steady-state values of the output were measured at each point (2 PSI steps, absolute value of the pressure reported) for 30 seconds. The pressure values range from 0 to 12 PSI (for the opening phase) and from 12 to 0 PSI (for the closing phase). The mean value was calculated at each point and graphed using MATLAB (R2023b; Mathworks).

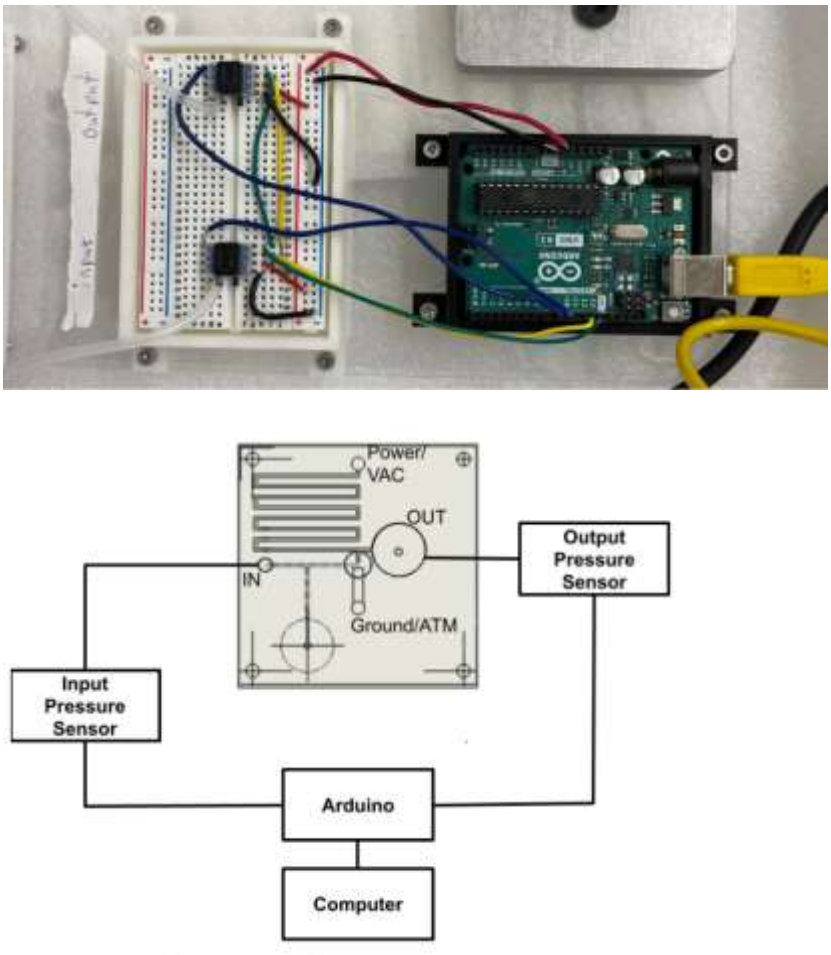

Fig 2.2. An Arduino Data Acquisition System. Transfer functions were measured by pressure sensors and an Arduino data acquisition system. Two independent pressure

transducers were used to measure applied input pressure and the corresponding output pressure.

For each valve (1- and 2-mm diameter), two inverter designs were developed and tested. In the first design, the pull-up resistor was a serpentine channel similar to the previous design utilized by Duncan et al. [2] and Werner et al. [8] (Fig 2.3B). The hydraulic resistance of the pull-up channel was approximately 16 times the resistance of the ground channel, exceeding the recommended minimum 10:1 ratio. In the second generation, the design was simplified (to minimize the total chip area and thus increase the gate density) to a straight channel (Fig 2.3B).

Compared to the serpentine channel, the straight channel was shorter by 59 mm (Fig 2.3B). However, by tuning both the width and depth of the channel, the resistance of the straight channel (4.46×10^{11} Pa · s/m^3) was analogous (ratio: 0.8) to the resistance of the serpentine channel (5.61×10^{11} Pa · s/m^3) (Table 6.1). The parameters of the ground channel were consistent and unchanged across the two designs. Two 4-mm valves were placed at the input and the output to act as indicators for inverting performance. Circular valves of 1 mm and 2 mm in diameter were tested in both designs since the membrane in bigger valves (3 and 4 mm) was prone to partial collapsing during the process based on preliminary data (APPENDIX A). In both designs, 2-mm valves exhibited more non-linear and distinguished gain that is useful for noise suppression of digital systems (Fig 2.3D). Compared to the serpentine design, the output pressure for the straight channels did not fully approach 0 (atmospheric pressure) as the input pressure is increased, implying an excess resistance in the ground channel or an insufficient resistance in the straight resistor (Fig 2.3D). Nevertheless, all four inverters showed a successful inverting of output from

the input signal that were demonstrated by the transfer functions and the inverting relationship of input and output indicator valves (Fig 2.3D). The successful implementation of inverters with the 3D printed strategy built the foundation for developing more complex (and useful) pneumatic digital systems via 3D printing.

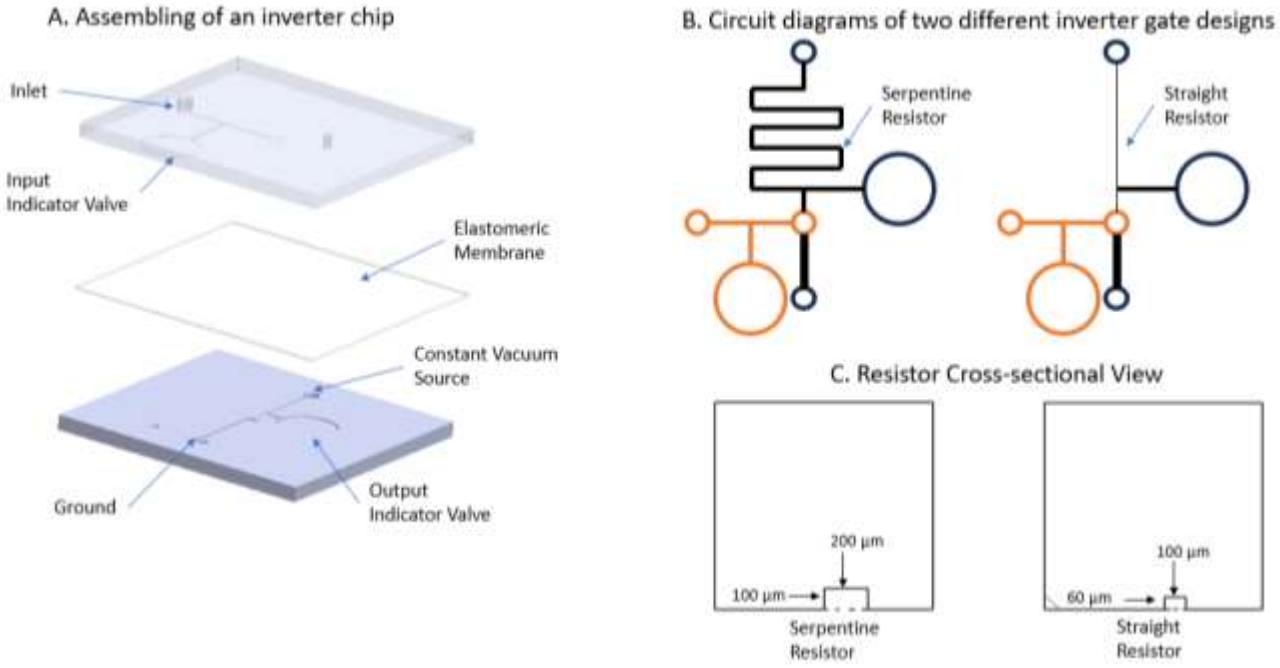

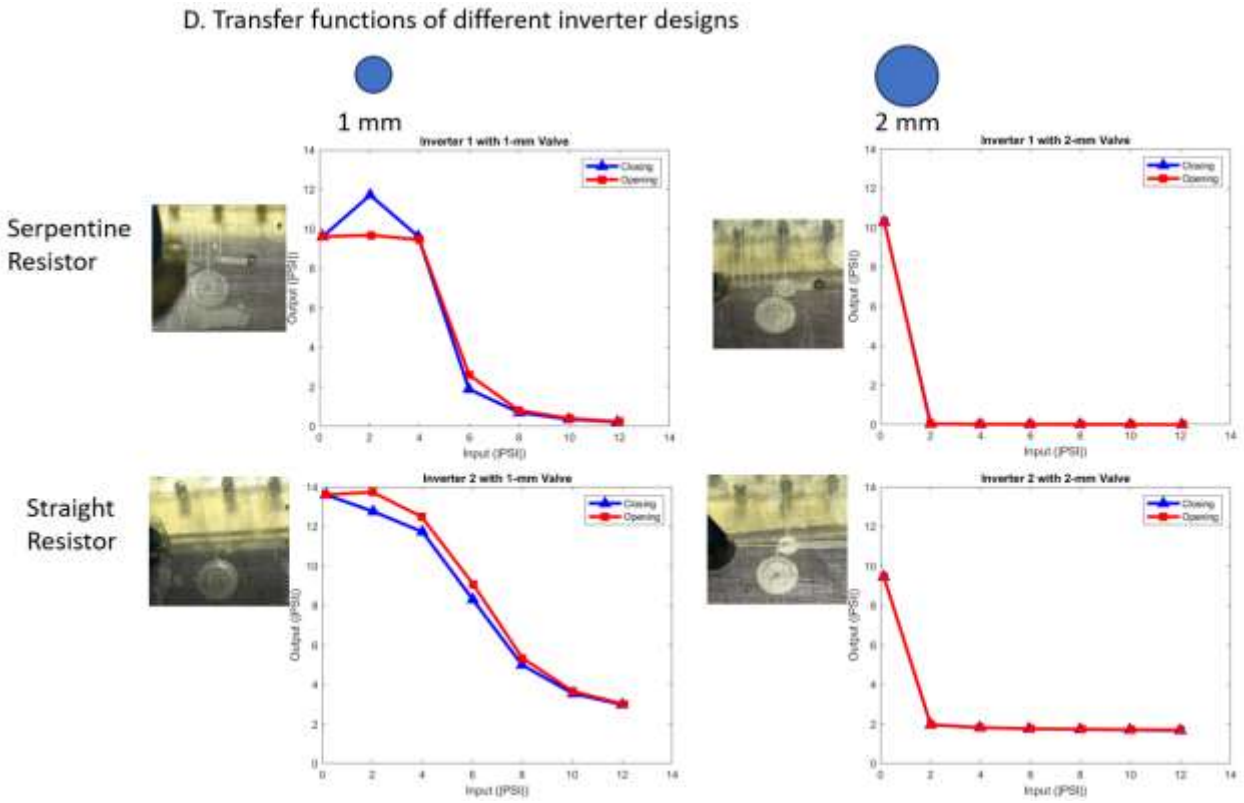

Fig 2.3. Inverting of Output from Input Signal. (A) Isometric view of an inverter chip. **(B)** Two different designs of pull-up resistors (black is the bottom layer, orange is the top layer). **(C)** Cross-sectional view of two resistor channels. **(D)** Transfer function of 4 different resistors: Serpentine channel with 1-mm valve, serpentine channel with 2-mm valve, straight channel with 1-mm valve, straight channel with 2-mm valve.

CHAPTER 3: Pneumatic 3-Ring Oscillator

After developing the 3D-printed inverter (the basic building block for pneumatic digital logic), we sought to develop circuits with more practical applications. A ring oscillator (that can be used as embedded self-priming pumps) is a simple and useful system that can be used to showcase the strength of the new fabrication strategy. An odd number of inverters can be connected in a closed loop to construct a ring oscillator (Fig. 3.1A). Each inverter in the circuit receives an input from the output of the previous inverter. A feedback channel is incorporated at the end of the chain (Fig. 3.1A) to close the loop. This mechanism creates an oscillation of signals in an infinite loop as long as power is provided to the system. A circular valve with a diameter of 2 mm was used to build the ring oscillator due to its non-linear and distinguished gain compared to a 1-mm circular valve. All pull-up resistors were located on the top layer of the device (Fig 3.1B). Each pull-up resistor was connected to a powerline with a cross-sectional area of 1 mm^2 to minimize excess resistance (Fig. 3.1B). All valves were located on the bottom layer along with the feedback loop (Fig. 3.1B). Via holes to connect signals between layers were placed at the end of each pull-up resistor (Fig 3.1B). To minimize excess resistance of the ground, the ground holes were directly placed onto the valve (Fig 3.1B). At the start of the experiment, air was blown into each ground hole to ensure that the membrane was not adhered to the HTL surface. Vacuum was constantly connected at the powerline of the chip. To examine the behavior of ring oscillators, a video recording approach was used (Fig 3.1C). To this end, videos were recorded using a Canon T1i DSLR camera (Canon Global). The first and last 10 seconds of all videos were cut using Adobe Express (Adobe Inc.) to remove any mechanical distortion when pressing the record button. All videos were converted to AVI using VLC

media player (VideoLAN). Using a previously developed approach [2], each frame in the videos was then processed by MATLAB to measure reflection of light from the valves. The mean intensity values of each frame were graphed using MATLAB as binary output in time domain. Oscillation frequencies were calculated by collecting all peak mean intensity values and dividing them by the total time using MATLAB.

Serpentine Channel Design

The serpentine inverter design was used to develop a 3D-printed ring oscillator. The signal of the serpentine ring oscillator started at the left inverter closest to the vacuum source and propagated from left to right (Fig 3.1C). The minimum vacuum to activate the device was approximately 4.0 PSI. The oscillation frequency increased as the vacuum increased. At 4.5 PSI, the oscillation frequency approached 0.7 Hz (Fig 3.1D). Oscillator frequencies were undetectable by the camera at higher vacuum.

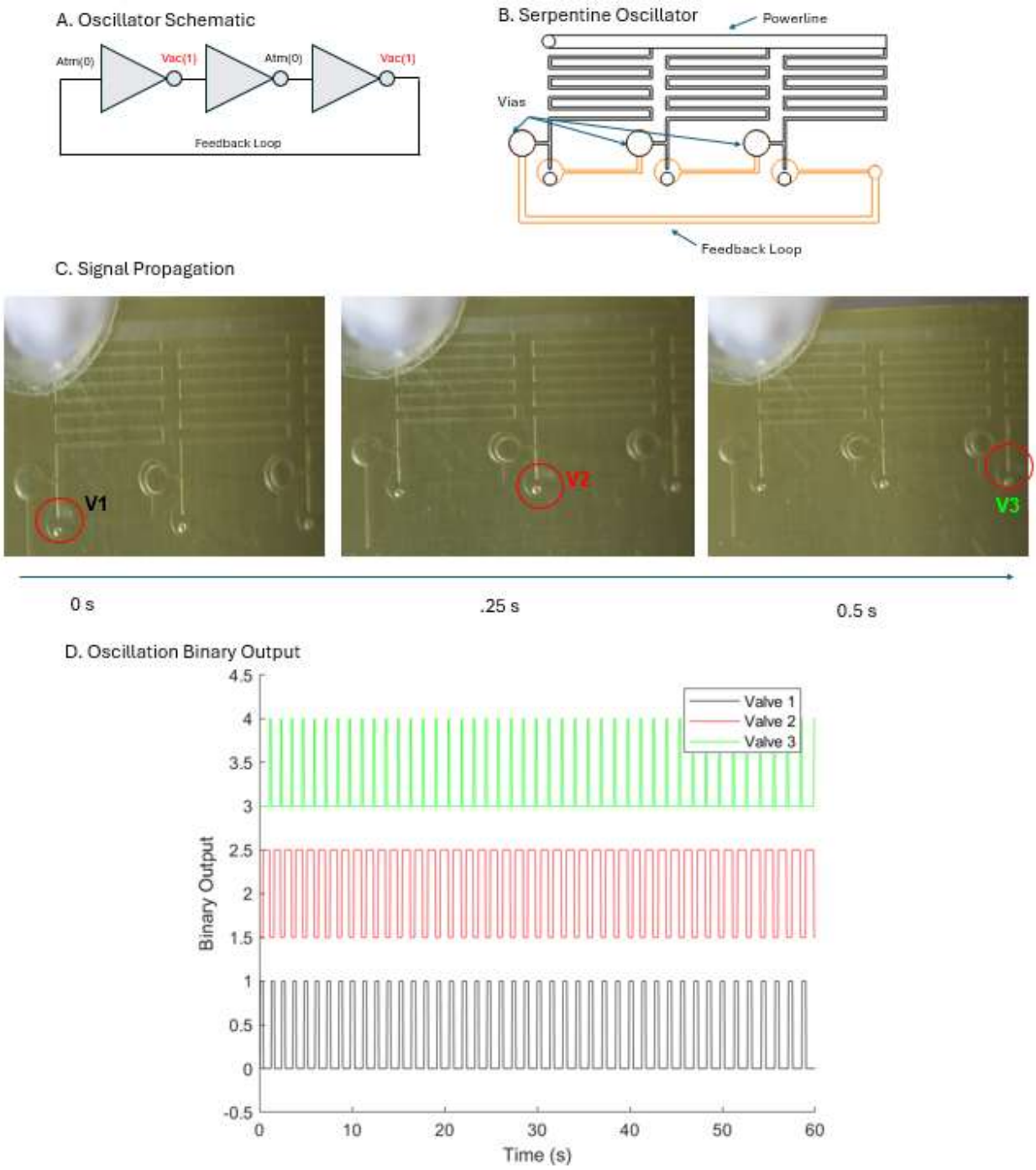

Fig 3.1. Serpentine Channel 3-Ring Oscillator (A) Schematic of a 3-ring oscillator, an infinite loop is established. **(B)** Using 3 serpentine inverter gates with a feedback loop to operate an oscillator. The top layer is black, and the bottom layer is orange. **(C)** Signal

propagation across 3 valves (V1, V2, V3) in time domain. **(D)** Binary output of valve actuation for each valve in 1 minute of oscillation.

Straight Channel Design

After establishing the ring oscillators with the previously established serpentine pull-up resistors, we sought to demonstrate a 3-ring oscillator by using the straight resistor design with a 2-mm valve (Fig 3.2A). The purpose of the experiment was to demonstrate the ability of the 3D printing approach to increase gate density. The ground hole was also placed directly upon the valves to reduce excess resistance in the ground channel (Fig 3.2A). Similar to the previous serpentine design, the signal also started at the left inverter closest to the vacuum source and propagated from left to right. The minimum vacuum to activate the device was also 4.0 PSI. At a vacuum of 4.5 PSI, the oscillation frequency approached 7.0 Hz, ten times higher than the previous design (Fig 3.2B). Ring oscillator frequencies were undetectable by the camera at higher vacuum. With the straight channel design, the occupancy area of the ring oscillator was decreased by a factor of 3.1, from 4.7 cm^2 down to 1.5 cm^2. It is noted that the shape of the straight channel can be altered to the serpentine design, further decreasing the occupancy area of the ring oscillator.

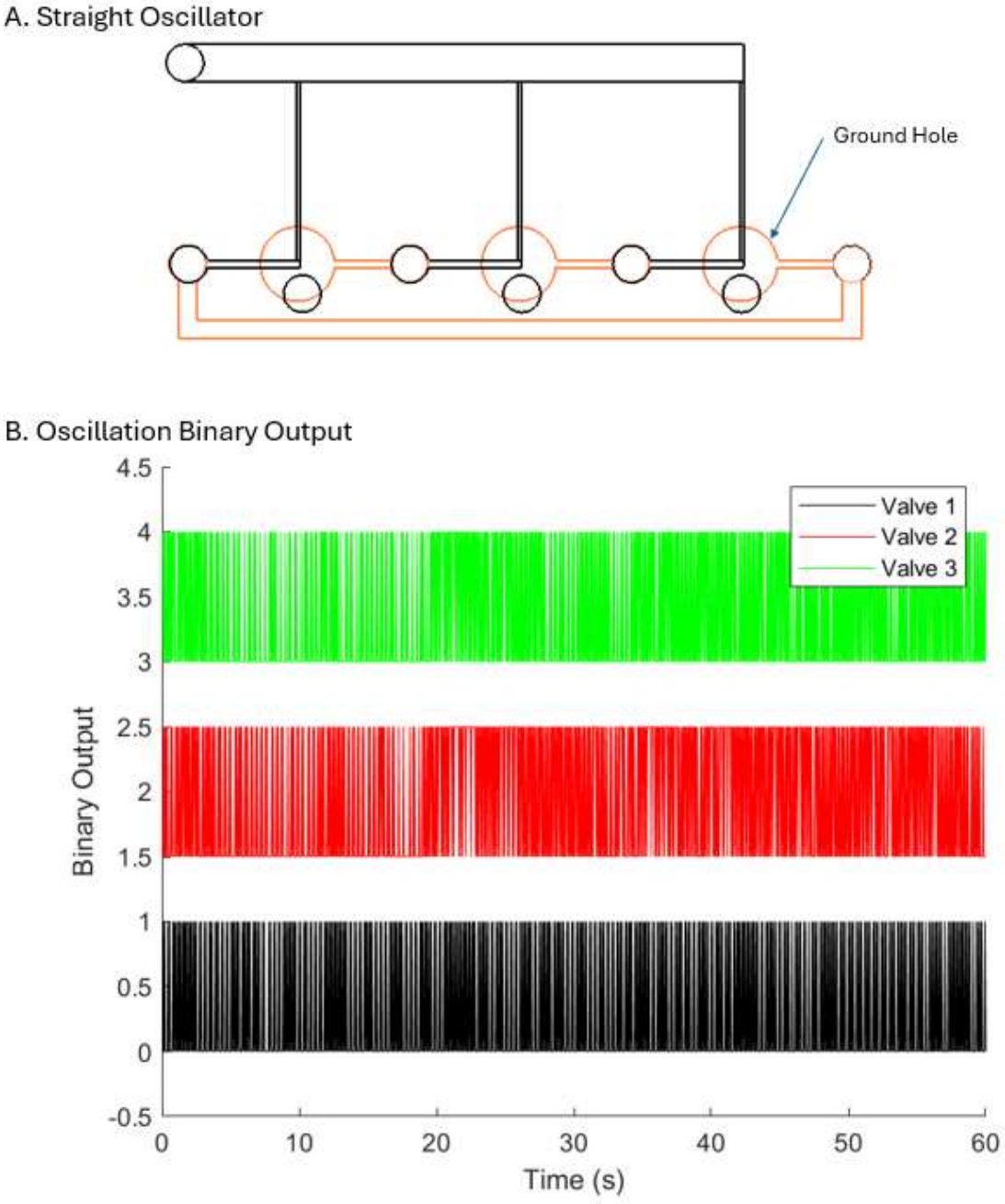

Fig 3.2. Straight Channel 3-Ring Oscillator (A) A simplified 3-ring oscillator with straight inverters. Black is the top layer and orange is the bottom layer. **(B)** Binary of output of three valves in one minute of oscillation.

CHAPTER 4: Peristaltic Pump Integration With a 3-Ring Oscillator

Next, ring oscillators were used to build microfluidic peristaltic pumps. To this aim, a 3-inverter ring oscillator was used. The outputs from each inverter were connected to three pump valves placed in series (Fig. 4.1A), similar to efforts by Duncan et al. (2). A channel with two reservoirs at each end was connected across the pump valves (Fig. 4.1A). The pump valves had the same design (2 mm in diameter) as the inverter valves (Fig. 4.1A). These valves actuate sequentially to produce a peristaltic pumping pattern transferring the fluid. To test the pump, the powerline of the ring oscillator was connected to the house vacuum system (WaterSaver Faucet Co.). A vacuum regulator (V-800-30W/K; AIRTROL) was used to control the applied input pressure to the pump. Input and output reservoirs were designed at the two ends of the fluid channel and via holes were punched at the reservoirs to access the fluid channel at the bottom layer. Air was blown into the fluid channel to unstick the valve membrane from the HTL surface prior to running the experiments. To test the pumps, a 10 μL solution (deionized water with food dye for visualization) was placed into the input reservoir via a micropipette before turning on the vacuum. Videos of the pump experiments were recorded using the Canon T1i DSLR camera (Canon Global). Volumetric flow rate was measured by slowing down videos by 0.25× using Clideo Video Editor (Clideo) to observe the flow of fluid across the channels. Time values were then input into MATLAB for analysis. At first, peristaltic pumping patterns were observed in earlier unsuccessful designs of the pump. However, the fluid traveled at a gradual rate until passing the first valve and failed to travel to the other side of the channel. The low pumping strength of the valve was caused by the high resistance (2.5×10^{11} Pa · s/m^3) of the connecting channels between the pump valves and the inverter gates. To

resolve the problem, the depth of the connecting channels was increased from 100 μm to 500 μm to decrease the resistance by a factor of 53 (from 2.5 x 10^{11} Pa · s/m to 4.7 x 10^{9} Pa · s/m^3). An improvement in the pump was observed as fluid was able to consistently travel across the channel (Fig. 4.1B). At 14 PSI, the 3-inverter system produced a pumping rate of 8.6 μL/sec (Figure C). Minimal changes were observed while decreasing the vacuum supply to 12 ($t(4) = 0.77$, $p = .48$) and 10 PSI ($t(4) = 0$, $p = 1.0$) (Fig. 4.1C). However, as the vacuum supply approached 8 PSI, the difference in pumping efficiency compared to 14 PSI became noticeable ($t(4) = 5.4$, $p = .0058$) (Fig. 4.1C). At times, dead volume remained along the channel that could only be cleared by maximizing the vacuum supply. The pump stopped functioning at around 6 PSI (Fig. 4.1C). A pressure of 10 PSI was concluded to be the benchmark for efficient pumping. Hydraulic resistance in the channel was reduced as the experiment went on due to the previous fluid priming of the channel, resulting in faster flow rates for the latter experiments.

A.

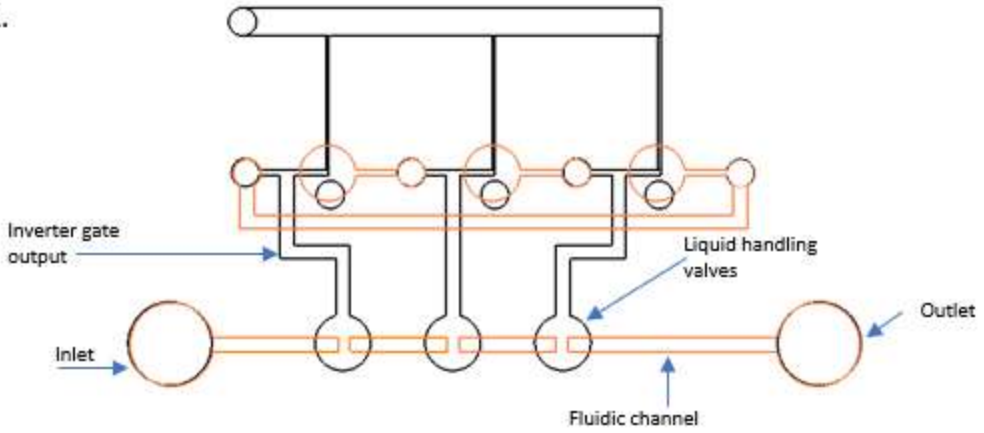
Inverter gate output
Liquid handling valves
Outlet
Inlet
Fluidic channel

B.

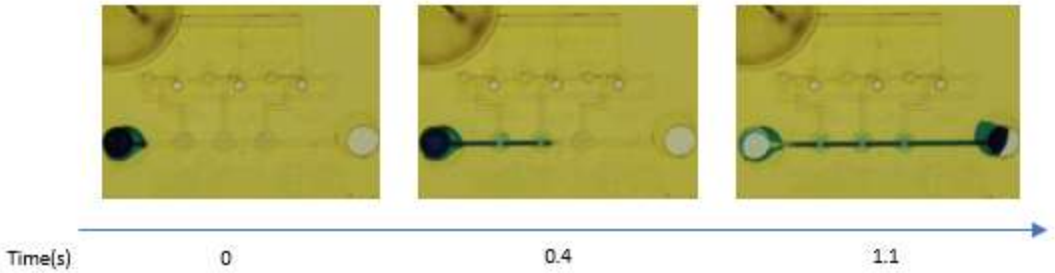
Time(s)
0
0.4
1.1

C.

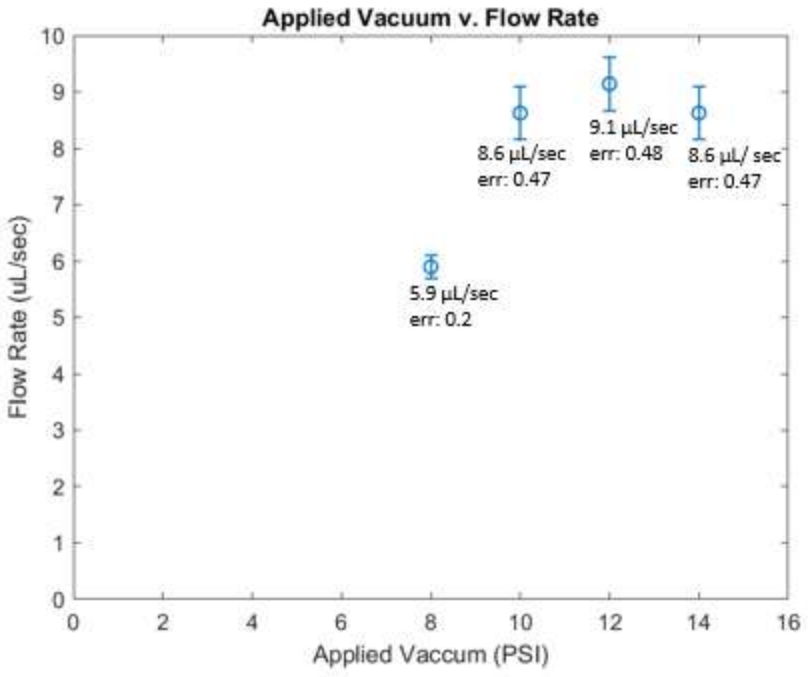
Applied Vacuum v. Flow Rate
Flow Rate (uL/sec)
Applied Vaccum (PSI)
8.6 µL/sec
err: 0.47
9.1 µL/sec
err: 0.48
8.6 µL/ sec
err: 0.47
5.9 µL/sec
err: 0.2

Fig 4.1. Peristaltic Pump Integration (A) Components of a peristaltic pump that is extended from the inverter gate outputs. The top layer is black. The bottom layer is orange. **(B)** Fluid is pumped across the channel in the time domain. **(C)** Mean flow rate with standard error bar at each vacuum value. The pump stopped operating at 6 PSI.

Incorporating Tubing and Reservoirs

The input and output reservoir design introduced multiple bubbles and dead volume which can be resolved by connecting the input and output of the system to external reservoirs via tubing (Fig 4.2A). Since the flow direction is left-to-right, a 15 mL centrifuge tube (containing water with trace dye) was placed on the left side while an empty 15 mL centrifuge tube was placed on the right side (Fig 4.2A). To seal off the connection, a cylindrical silicone cabinet bumper (DAMPONE) was adhered to the input and output (Fig 4.2A). Each bumper was punctured using a 2.00 mm Uni-Core Punch (Qiagen Group) for tubing connection. The initial volume inside the input reservoir was recorded before each experiment. To maximize pump efficiency, the pressure was set at 14 PSI throughout each experiment. Each experiment was run for 1 minute before the final volume inside the input reservoir was recorded (Fig 4.2B). The flow rate for each experiment was recorded accordingly (Fig 4.2C). The mean flow rate was 0.57 mL/min (9.5 μL/sec) (Fig 4.2C). Noticeable leaks were observed between the chip and the silicone bumpers after a couple minutes of running the experiment due to delamination of the adhesive bumper (Fig 4.2B). To resolve this problem for future experiments, PDMS can be compressed onto the input and output from both sides using two pieces of acrylic that are held together via screws.

A.

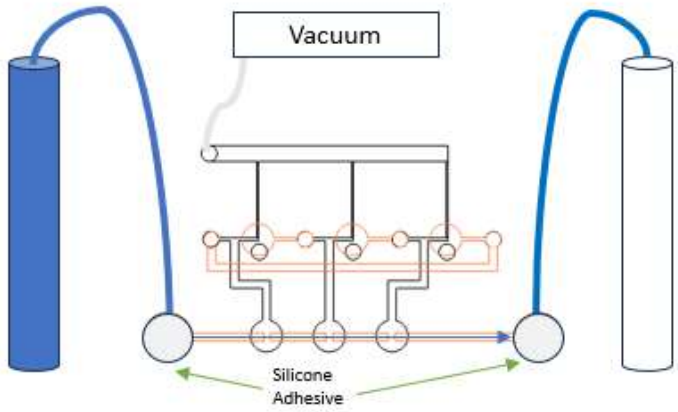

B.

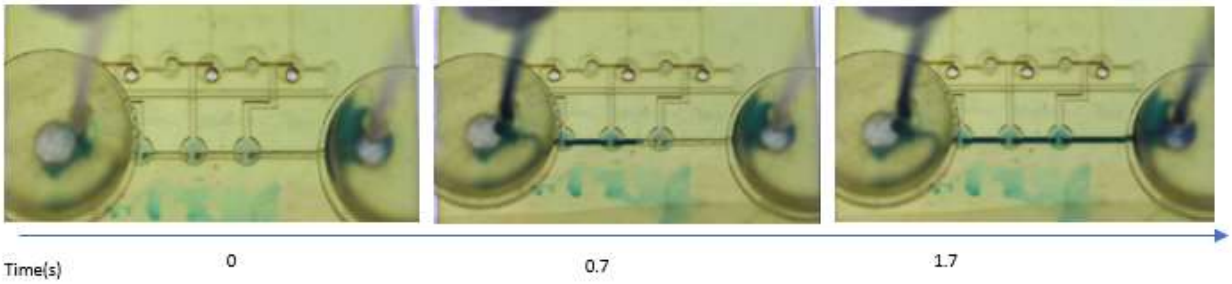

C.

Experiment	Pressure (|PSI|)	Time (seconds)	Initial Volume (ml)	Final Volume (ml)	Volume Pumped(ml)	Flow Rate
1	14	60	12.1	11.5	0.6	0.6 ml/min
2	14	60	10.9	10.3	0.6	0.6 ml/min
3	14	60	10	9.5	0.5	0.5 ml/min
Mean Flow Rate	0.57 ml/min					
Standard Error	0.03					

Fig 4.2. Incorporating Tubing and Reservoirs (A) Set up of a peristaltic pump with 2 centrifuge tube reservoirs, silicone adhesives are used to seal the connections. **(B)** Operation of the pump set up in time domain. **(C)** Constant operation of peristaltic valve in 1-minute experiments.

CHAPTER 5: Vertical Design of Inverters and 3-Ring Oscillators

Prior designs in this effort along with previous efforts developed pneumatic logic channel designs and features along the 2-dimensional plane (XY). While being the most straightforward and simple approach, planar designs limit the available workspace that can be used to minimize the overall gate densities. By taking advantage of SLA 3D-printing, development of vertical channels, inverters, and ring oscillators was investigated. Channel features were designed in the Z-direction around the region where the valves resided (Fig. 5.1A). The pull-up resistor with a cross-section of 200 × 200 μm was placed in the Z-direction, perpendicular to the valve seat (Fig. 5.1A). The length of the channel was 1.65 mm, extending vertically from the powerline to the membrane (Fig. 5.1A). The powerline was designed above the valves, extending along all resistor channels in the system (Fig. 5.1C). On the other side of the chip, the feedback loop was also converted vertically, extending along all valve seats in the system (Fig 5.1C). Connections between valves along with via holes were kept the same at this stage (Fig 5.1C). To achieve all the above, the thickness of each part was increased to 2 mm.

The vertical inverter design exhibited nonlinear and distinguished gain (Fig. 5.1B). The valve was easily opened at a low vacuum (Fig. 5.1B). Atmospheric pressure was completely dominant over the output of the inverter starting at 4 PSI (Fig. 5.1B).
The same peristaltic pumping system was integrated into the circuit to compare its performance with earlier designs (Fig. 5.1D). For each experiment, a 10 μL solution (food dye mixed inside deionized water) was placed into the input reservoir via a micropipette before turning on a desirable vacuum. At 14 PSI, the flow rate was 9.8 μL/sec (SE: 0.67) (Fig. 5.1E). The flow rate wasn't significantly changed when tuning the vacuum to 12 PSI (*t*

(4) = 0.96, p = .046), 10 PSI (t (4) = 0.42, p =.70), 8 PSI (t (4) = 0.90, p = .42) (Fig. 5.1E). A significant decrease in volumetric volume rate was shown when tuning the vacuum down to 6 PSI (t (4) =3.1, p = .037) (Fig. 5.1E). The pump stopped operating when the vacuum approached 4 PSI (Fig. 5.1E). A decrease in hydraulic resistance was again observed in this experiment. Compared with the pump operated by the straight channel ring oscillator, there are no significant differences in volumetric flow rate at 14 PSI (t (4) = 1.4, p = .24) and 12 PSI (t (4) = 2.6, p = .058). The vertical pump has a significantly higher volumetric flow rate than the straight channel pump at 10 PSI (t (4) = 4.5, p = .011) and 8 PSI (t (4) = 3.2, p = .032). At 6 PSI, the straight channel pump stopped functioning while the vertical channel pump continued to operate. With a decrease in occupancy area by a factor of 3.7 (from 1.5 cm^2 to 0.4 cm^2), the vertical pump achieved the same volumetric flow rate at vacuum above 12 PSI and a more efficient volumetric flow rate at vacuum below 12 PSI, making it a more favorable pump between the two.

A. Vertical Inverter Design

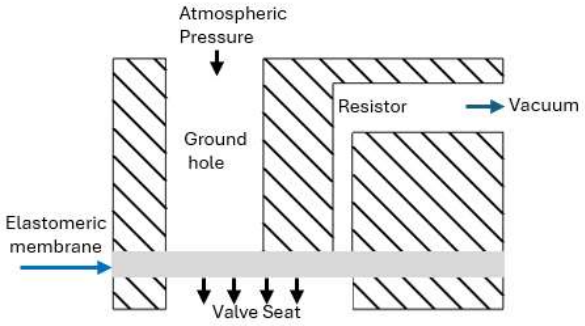

B. Transfer Function

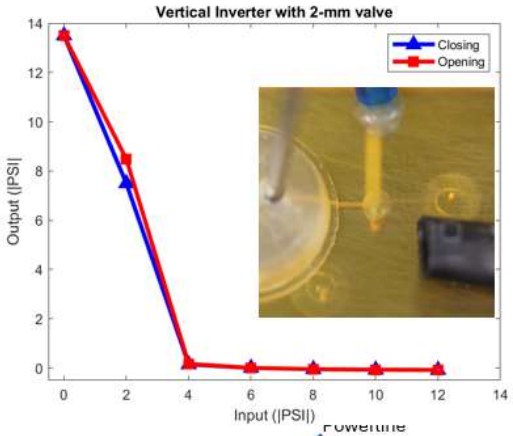

C . Vertical Oscillator Schematic

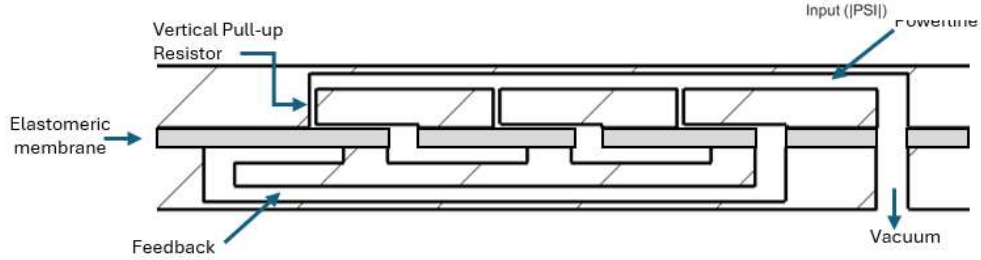

D. Vertical Oscillator Pump Integration

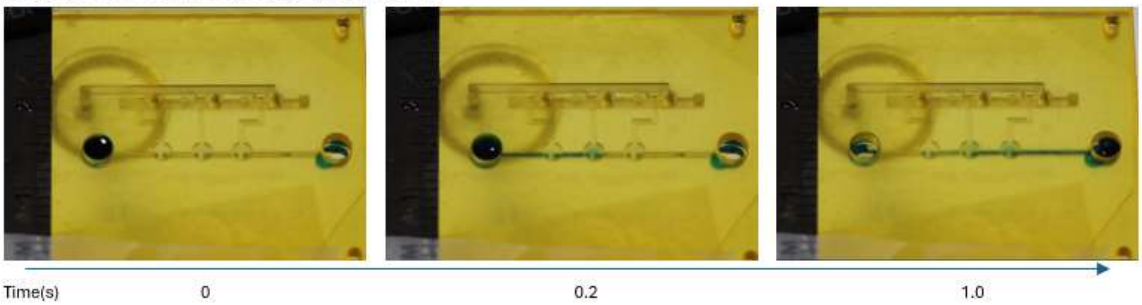

E.

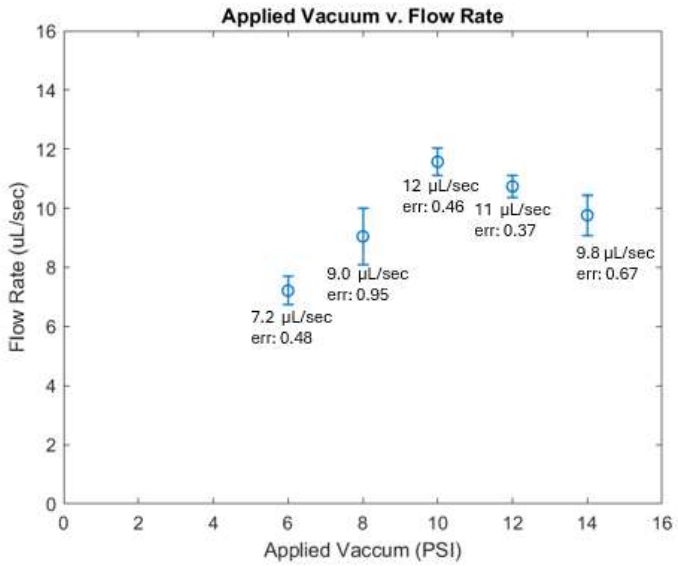

Fig 5.1. Vertical Design of a 3 Ring-Oscillator Pump (A) Cross-sectional view of a vertically designed inverter. **(B)** Transfer function of a vertical inverter with 2-mm valve**.** **(C)** Three vertical inverters along with a vertical ground hole are connected in a loop to form a pneumatic ring oscillator. **(D)** Utilizing the vertical ring oscillator to operate a peristaltic pump. **(E)** Mean flow rate with standard error bar at each vacuum value. The pump stopped operating at 4 PSI.

CHAPTER 6: Discussion

By tuning with channel's cross-sectional parameters and employing the vertical design of chip features, the final circuit density (7.01 gate/cm^2) was increased by 10 times the original density (0.687 gate/cm^2). High-resolution (20 μm) stereolithographic 3D printing was implemented to design and develop vacuum-based pneumatic logic systems, capable of pumping liquids up to 11.6 μL/sec across a fluid channel (channel dimension: $500 \times 500 \times 23200$ μm). Using tubing and silicone adhesives, an automated peristaltic pumping system with reservoirs at both ends was demonstrated, which is useful for prolonged and stabilized handling of large volumes of fluid. Smaller valves can be introduced to the system to accommodate more gates to the circuit, which is advantageous for designing complex digital systems. Since the alignment of gates in this study was linear, rearrangement of gates to other formations (e.g. circle) similar to Duncan et al. is highly promising to further increase the gate density [5].

A simplified version of the Navier-Stokes equation was used to compute the hydraulic resistance of rectangular microchannel when $h/w \ll 1$ [11]. The dynamic viscosity (μ) of air at 20°C is 1.80 x 10^{-5} Pa · s [8]. Although the condition didn't fully apply to the designs in this effort, the values calculated here acted as useful approximations.

$$R_{rec} = \frac{1}{1 - 0.63\left(\frac{h}{w}\right)} \frac{12\mu L}{h^3 w}$$

Table 6.1. Parameters of Different Inverter Designs					
Design	Width (w) (μm)	Height (h) (μm)	Length (L) (μm)	R_{rec} ($Pa \cdot s/m^3$)	Density
Serpentine	200	100	64000	5.61×10^{11}	.687 gates/cm^2
Straight	100	60	5000	4.46×10^{11}	1.96 gates/cm^2
Vertical	200	200	1650	4.05×10^{9}	7.01 gates/cm^2

Scaling of SLA 3D-printed pneumatic logic chip is complicated by the presence of uncured resin inside the vertical resistor channels and the powerline that is connected to them. The problem was resolved by injecting air and isopropyl alcohol across the channels to export the uncured resin. However, this method is not reliable when the hydraulic resistance of the channels is too high, resulting in trapped uncured resin inside the channels.

Fused deposition modeling (FDM) 3D printing had been used in Conrad et al. to adapt soft-lithographic digital pneumatic logic for controlling soft robotic actuators [12]. Soft-lithographic digital pneumatic logic's high-pressure tolerance is promising for driving large soft robots. However, soft-lithographic valve's large membrane dimensions along with their intricate designs limit their applications in complex and miniaturized pneumatic logic circuits [12]. Conrad et al. utilized a positive pressure-driven approach, which can introduce leakage if the supplied pressure and duration exceed its tolerance. In addition, FDM 3D printing's ability to create airtight bonds among layers is often limited [12]. It is

because FDM 3D printing relies on mechanical bonds to adhere their layers. In contrast, SLA 3D printing relies on chemical bonds to create isotropic parts [13]. As a result, SLA 3D-printed parts are highly water and airtight, ensuring the durability and reliability of logic chips and fluidic handling devices. Normally close monolithic valves are also more suitable for large-scale, complex integration of high-throughput devices due to their simple design [3].

Further investigation is needed to fully explore the potential of SLA 3D-printed pneumatic logic. Since chip real estate is often limited in microfluidic devices, it is necessary to constrain integrated controllers while achieving the desired complexity of microelectronic systems. By leveraging the inherent advantages of pneumatic digital systems, coupled with the design freedom of SLA 3D printing, advances in miniaturized soft robotics and pneumatic computers can be enabled to compete with their electronic counterparts.

References

[1] Brower, K., Puccinelli, R. R., Markin, C. J., Shimko, T. C., Longwell, S. A., Cruz, B., Gomez-Sjoberg, R., & Fordyce, P. M. (2018). An open-source, programmable pneumatic setup for operation and automated control of single- and multi-layer microfluidic devices. HardwareX, 3, 117–134.

[2] Duncan, P. N., Nguyen, T. V., & Hui, E. E. (2013). Pneumatic oscillator circuits for timing and control of integrated microfluidics. Proceedings of the National Academy of Sciences of the United States of America, 110(45), 18104–18109.

[3] Grover, W. H., Skelley, A. M., Liu, C. N., Lagally, E. T., & Mathies, R. A. (2003). Monolithic membrane valves and diaphragm pumps for practical large-scale integration into glass microfluidic devices. Sensors and Actuators B: Chemical, 89(3), 315–323.

[4] Ahrar, S., Raje, M., Lee, I. C., & Hui, E. E. (2023). Pneumatic computers for embedded control of Microfluidics. Science Advances, 9(22).

[5] Duncan, P. N., Ahrar, S., & Hui, E. E. (2015). Scaling of pneumatic digital logic circuits. Lab on a Chip, 15(5), 1360–1365.

[6] Devaraju, N. S., & Unger, M. A. (2012). Pressure driven digital logic in PDMS based microfluidic devices fabricated by multilayer soft lithography. Lab on a Chip, 12(22), 4809.

[7] Hoang, S., Karydis, K., Brisk, P., & Grover, W. H. (2021). A pneumatic random-access memory for controlling soft robots. PLOS ONE, 16(7).

[8] Werner, E. M., Lam, B. X., & Hui, E. E. (2022). Phase-Optimized Peristaltic Pumping by Integrated Microfluidic Logic. *Micromachines*, *13*(10), 1784.

[9] Kamperman, T., Moreira Teixeira, L., Salehi, S. S., Kerckhofs, G., Guyot, Y., Geven, M., Geris, L., Grijpma, D., Blanquer, S., & Leijten, J. (2020). Engineering 3D parallelized

microfluidic droplet generators with equal flow profiles by computational fluid dynamics and stereolithographic printing.

[10] Carnero, B., Radziunas-Salinas, Y., Rodiño-Janeiro, B. K., Ballesta, S. V., & Flores-Arias, M. T. (2024). Versatile hybrid technique for passive straight micromixer manufacturing by combining pulsed laser ablation, stereolithographic 3D printing and computational fluid dynamics. Lab on a Chip, 24(1), 2669–2682.

[11] Rousset, N., Lohasz, C., Boos, J. A., Misun, P. M., Cardes, F., & Hierlemann, A. (2022). Circuit-Based Design of Microfluidic Drop Networks. Micromachines, 13(7), 1124.

[12] Conrad, S., Teichmann, J., Auth, P., Knorr, N., Ulrich, K., Bellin, D., Speck, T., & Tauber, F. J. (2024). 3D-printed digital pneumatic logic for the control of soft robotic actuators. Science robotics, 9(86), eadh4060.

[13] FDM vs. SLA: Compare filament and resin 3D printers. Formlabs. (n.d.).

APPENDIX A: Pneumatic Valve Fluidic Visualization

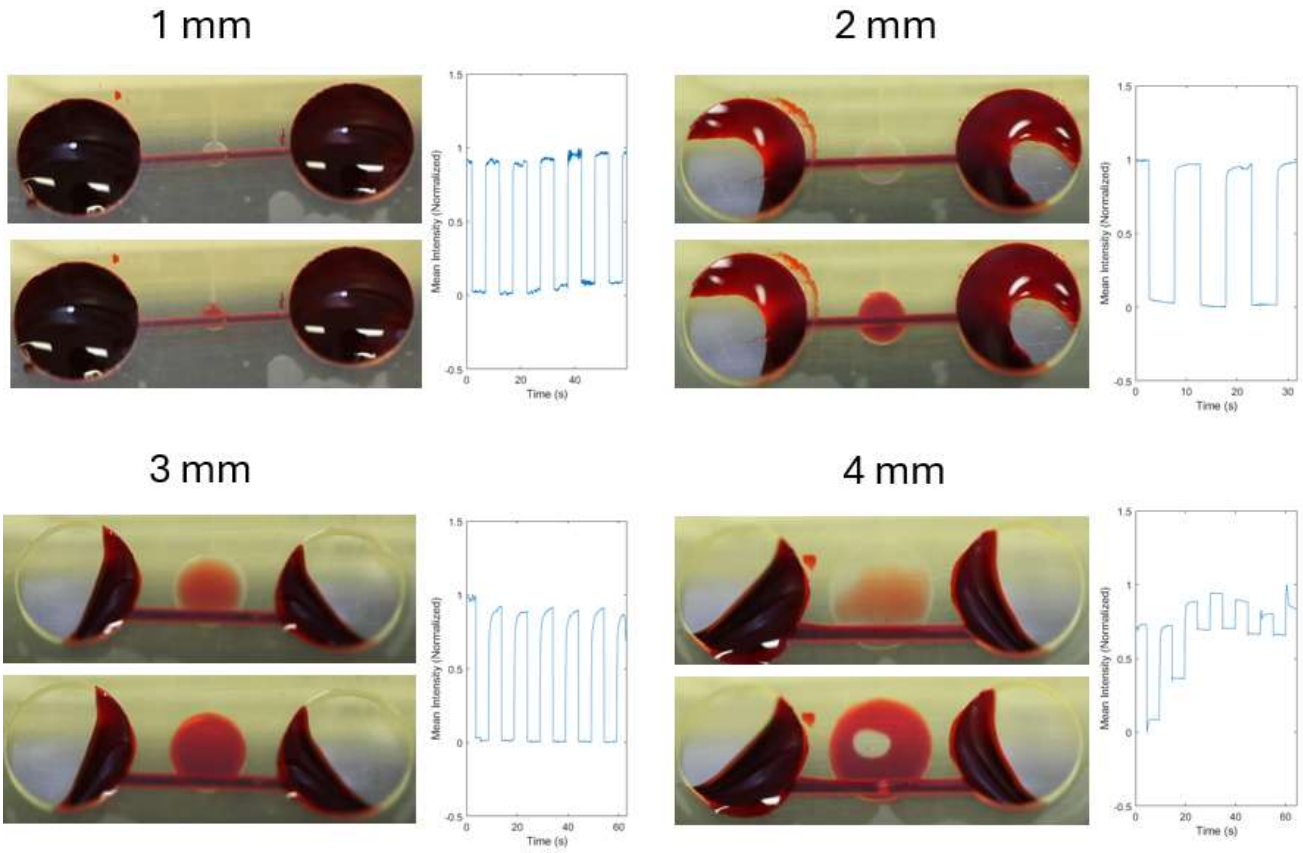

Four circular valves with different diameters (1 mm, 2 mm, 3 mm, 4 mm) were tested for functional actuation. All valves had a channel height of 0.1 mm. The valve lied in the middle of a channel that had 2 fluid reservoirs. For a minute, each valve was continuously actuated for 5 seconds before they were closed for 5 seconds. When opened, fluid from the channel filled up the volume of the valve seat to provide a visual illustration of valve actuation. Mean intensity values were taken from the videos and plotted against time. Dead volumes were observed in 3-mm and 4-mm valves. In conclusion, 1-mm and 2-mm valves showed promising actuation results and were later used in inverter designs.

APPENDIX B: Polishing HTL Chips Using Commercial Products

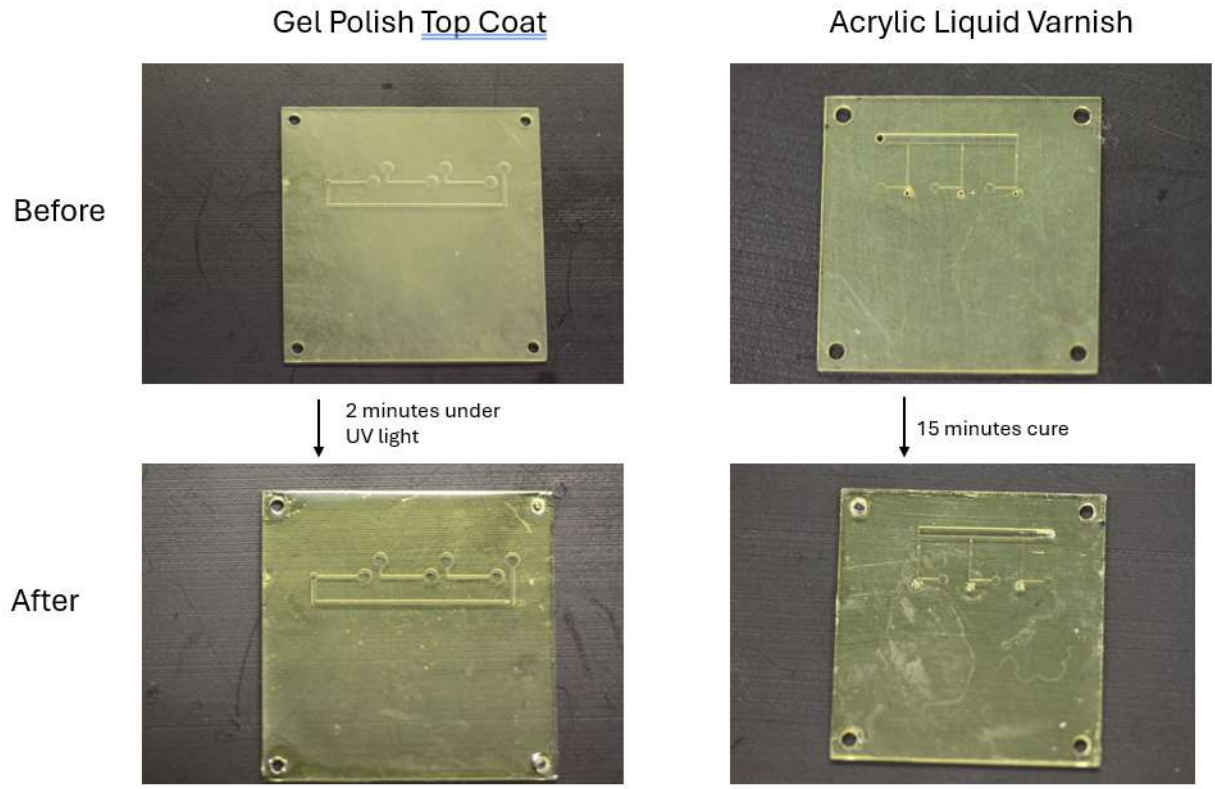

The bottom surface of each chip was opaque due to the scratches that were observed on the platform. To resolve this issue, two coating products were tested for its interaction with the HTL surface. Gel top coat for nail polish was coated onto the non-feature layer of the chip and allowed to polymerize under UV light for 2 minutes. Visual differences were observed after using gel polish top coat. Scatches were mostly eliminated, and the chip became more translucent. Acrylic liquid varnish used in canvas painting was also investigated. Acrylic liquid varnish was applied onto the non-feature layer and allowed to cure for 15 minutes. Translucency was increased after 15 minutes but was inadequate when it was compared to gel polish top coat. As a result, gel top coat was selected as the polishing product for the chips in this research.